COMPUTER-AIDED CIVIL AND INFRASTRUCTURE ENGINEERING

Computer-Aided Civil and Infrastructure Engineering **29** (2014) 738–757

Identifying the Modal Parameters of a Structure from Ambient Vibration Data via the Stationary Wavelet Packet

W. C. Su

National Center for High Performance Computing, National Applied Research Laboratories, Hsinchu 30050, Taiwan

C. S. Huang*

Department of Civil Engineering, National Chiao Tung University, Hsinchu 30050, Taiwan

C. H. Chen

Department of Civil and Environment Engineering, National University of Kaohsiung, Kaohsiung 81148, Taiwan

C. Y. Liu, H. C. Huang & Q. T. Le

Department of Civil Engineering, National Chiao Tung University, Hsinchu 30050, Taiwan

Abstract: *Ambient vibration tests are conducted widely to estimate the modal parameters of a structure. The work proposes an efficient wavelet-based approach to determine the modal parameters of a structure from its ambient vibration responses. The proposed approach integrates the time series autoregressive (AR) model with the stationary wavelet packet transform. In addition to providing a richer decomposition and allowing for an improved time–frequency localization of signals over that of the discrete wavelet transform, the stationary wavelet packet transform also has significantly higher computational efficiency than the wavelet packet transform in terms of decomposing time-shifted signals because the former has a time-invariance property. The correlation matrices needed in determining the coefficient matrices in an AR model are established in subspaces expanded by stationary wavelet packets. The formulation for estimating the correlation matrices is shown for the first time. Because different subspaces contain signals with different frequency subbands, the fine filtering property enhances the ability of the proposed approach to identify not only the modes with strong modal interference, but also many modes from the responses of very few measured degrees of freedom. The proposed approach is validated by processing the numerically simulated responses of a seven-floor shear building, which has closely spaced modes, with considering the effects of noise and incomplete measurements. Furthermore, the present approach is employed to process the velocity responses of an eight-storey steel frame subjected to white noise input in a shaking table test and ambient vibration responses of a cable-stayed bridge.*

*To whom correspondence should be addressed. E-mail: *cshuang@mail.nctu.edu.tw*.

1 INTRODUCTION

Capable of reflecting the dynamic characteristics of a structure, modal parameters identified from its measured dynamic responses can offer a valuable reference to efforts to update structural design models (García-Palencia and Santini-Bell, 2013; Lozano-Galant et al., 2013) and perform vibration control (Adeli and Saleh, 1997; Kang et al., 2012), health monitoring (Yuen and Katafygiotis, 2006; Soyoz and Feng, 2009; Hu et al., 2013), and damage assessment (Jiang and Adeli, 2007; Osornio-Rios et al., 2012) of a particular structure. Identification of modal parameters from dynamic responses can be carried out in either the frequency, time or time–frequency domains. The development of typical

DOI: 10.1111/mice.12115

approaches of system identification in the frequency and time domains can be found in many text books (i.e., Ljung, 1999; Schoukens and Pintelon, 1991). Recently, Sirca and Adeli (2012) provided an excellent review of representative works on structural system identification published in journals since 1995. The paper includes 191 references and classifies the methods of system identification as conventional model-based approaches, biologically inspired approaches, signal processing based approaches, chaos theory, and multiparadigm approaches.

Owing to its flexibility, ambient vibration test is often undertaken to attain the required dynamic responses of a structure. Because the excitation for ambient vibrations includes natural forces (e.g., wind, tidal waves, and earthquakes tremors), the input forces are too complicated to measure. Numerous algorithms have been developed to identify modal parameters of a structure from its ambient vibrations. These algorithms work in either the frequency, time or time-frequency domains. Although generally simple, the methods in the frequency domain (Bendat and Piersol, 1993; Yan and Ren, 2012) do not work well for structural systems with heavy damping and strong modal interference (Lardies and Ta, 2011).

In the time domain, the random decrement technique (Cole, 1971; Vandiver et al., 1982; Huang and Yeh, 1999) is typically applied to convert ambient vibration responses into free decay responses, which are also called Randomdec signatures. The modal parameters from the free decay responses are then identified by using either the Ibrahim time-domain scheme (Ibrahim and Mikulcik, 1973; Ibrahim and Pappa, 1982) or the least-squares complex exponential method (Brown et al., 1976; Vold and Russell, 1983). Although the input forces are assumed to be white noise, Huang and Yeh (1999) demonstrated theoretically that the Randomdec signatures converted from velocity or displacement responses of a system are equivalent to the free decay responses of the system, whereas Randomdec signatures converted from acceleration responses are not. The ambient vibration responses are also often processed directly using the time series models, autoregressive (AR) (Wang and Fang, 1986; Huang, 2001; Liu et al., 2011) and autoregressive moving average (ARMA) (Loh and Wu, 1996; Lardies, 2010), stochastic subspace approaches (Huang and Lin, 2001; Ali and Okabayashi, 2011; He et al., 2008), natural excitation technique with the eigensystem realization algorithm (NExT-ERA) (Dionysius and Yozo, 2007; Caicedo, 2011), and blind source separation methods (Zhou and Chelidze, 2007; Mcneil, 2011; Hazra et al., 2012). The input forces for ambient vibration responses of structures are assumed to be white noise in the AR model, stochastic subspace approaches and NExT-ERA; this assumption is quite acceptable in civil engineering applications. The ARMA model and blind source separation methods do not make such a strict assumption and are more complicated than the AR model, stochastic subspace approaches and NExT-ERA.

Wavelet transformations provide time–frequency analyses and offer alternative signal analysis methods by presenting information in the time and frequency domains simultaneously. Wavelet transformations were first applied to structural system identification about two decades ago. Discrete wavelet transforms (Robertson et al.,1998; Huang et al., 2005), wavelet packet transforms (Jiang and Adeli, 2004; Jiang et al., 2007; Chen et al., 2013), continuous wavelet transforms (Schoenwald, 1993; Ruzzene et al., 1997; Gouttebroze and Lardies, 2001; Kougioumtzoglou and Spanos, 2013; Hsu, 2013), and wavelet neural networks (Hung et al., 2003; Jiang and Adeli, 2005, 2008; Adeli and Jiang, 2006, 2009; Lin et al., 2012; Kodogiannis et al., 2013) were employed to system identifications using the dynamic responses and inputs of structures or the free vibrations of structures.

Wavelet-based approaches and Hilbert transform methods are also particularly used for identifying modal parameters of a structure from its ambient vibration responses. Most of these approaches collaborate with the random decrement technique. To determine the modal parameters from the Randomdec signatures, Yang et al. (2004) employed Hilbert–Huang transform (Huang et al., 1998), whereas Lardies and Gouttebroze (2002) proposed a method based on the wavelet ridges of continuous Morlet wavelet transform. Yang and Miyamoto (2006) presented a comparative study of estimating modal parameters from Randomdec signatures by using the approach of Lardies and Gouttebroze (2002) and the improved Hilbert–Huang transform. In another comparative study, Lardies and Ta (2011) determined the modal parameters of a cable-stayed bridge by using a modified approach of Lardies and Gouttebroze (2002) and a subspace algorithm. Based on the approach of Huang and Su (2007), which combines the autoregressive with exogenous input (ARX) model with the continuous wavelet transform and was developed to identify the modal parameters of a structure under an earthquake, Chen and Ou (2011) processed the ambient vibration responses of a cable-stayed bridge. Without using the random decrement technique, Hazra and Narasimhan (2010) directly determined the modal parameters of a building from its ambient vibration responses by using an approach that combines second-order blind identification technique with the stationary wavelet transform. Notably, the approaches, which

were developed for processing the forced and free vibration responses, are theoretically applicable to process the Randomdec signatures. Nevertheless, the reference degree of freedom chosen to construct the Randomdec signatures may significantly affect the accuracy of modal parameters identified from the Randomdec signatures. In addition to that, the ambient vibrations are converted into free decay responses with a relatively short duration, and the edge effect in the wavelet transform can have considerable effects on accurately determining the modal parameters.

This work develops a novel approach in the time–frequency domain without the assistance of the random decrement procedure. The proposed approach combines the AR model and the stationary wavelet packet transform. The measured ambient vibration responses of a structure are expanded by the stationary wavelet packets, and the correlation functions among the measured degrees of freedom are estimated in the needed subspaces expanded by stationary wavelet packets. Notably, the correlation matrices in the stationary wavelet packet space is formulated herein for the first time in literature. Then, the coefficient matrices in the AR model are simply estimated using a traditional least-squares scheme. Modal parameters of the structure are directly determined from those coefficient matrices. The fine filtering property in the stationary wavelet packet transform enhances the ability of the proposed approach to identify not only the modes with strong modal interference, but also many modes from the responses of very few measured degrees of freedom. Validity of the proposed approach is verified by processing the numerically simulated responses of a seven-degrees-of-freedom system, which has closely spaced modes, with considering the effects of noise and incomplete measurements. Furthermore, the proposed approach is applied to process the velocity responses of an eight-storey steel frame subjected to white noise input in the shaking table tests and the ambient vibration responses of a cable-stayed bridge with a main span of 330 m and a side span of 180 m.

2 METHODOLOGY

2.1 AR model

As is well known, the ambient vibration responses of a system can be described by the AR model with the order I, denoted by AR(I), which is mathematically expressed as

$$\mathbf{y}(t) = \sum_{i=1}^{I} \Phi_i \mathbf{y}(t-i) + \mathbf{a}(t) \tag{1}$$

where $\mathbf{y}(t-i)$ is the measured velocity response vector at time $t - i\Delta t$; $1/\Delta t$ is the sample rate of measurement; Φ_i is coefficient matrix; and $\mathbf{a}(t)$ belongs to a vector white-noise process with the following properties

$$E[\mathbf{a}(t)] = \mathbf{0} \quad \text{and} \quad E[\mathbf{a}(t-i)\,\mathbf{a}^T(t-j)] = \delta_{ij}\mathbf{W} \tag{2}$$

where $E[]$ denotes the mean-value operation, δ_{ij} represents the Kronecker symbol, and $\mathbf{W}$ is the covariance matrix of $\mathbf{a}(t)$.

Multiplying $\mathbf{y}^T(t-k)$ by both sides of Equation (1), taking the mean values and using the fact that $E[\mathbf{a}(t)\mathbf{y}^T(t-k)] = \mathbf{0}$ yield the following relationship

$$\mathbf{R}(-k) = \sum_{i=1}^{I} \Phi_i \mathbf{R}(i-k) \tag{3}$$

where $\mathbf{R}(k) = E[\mathbf{y}(t)\mathbf{y}^T(t+k)]$. Applying $\mathbf{R}(-k) = \mathbf{R}^T(k)$ to Equation (3) yields

$$\mathbf{R}^T(k) = \sum_{i=1}^{I} \Phi_i \mathbf{R}^T(k-i) \tag{4}$$

By using different k in Equation (4), the following equation can be derived from Equation (4):

$$\hat{\mathbf{R}} = \tilde{\mathbf{R}}\tilde{\Phi} \tag{5}$$

where

$$\hat{R} = \left[\mathbf{R}^T(k_i+1)\ \mathbf{R}^T(k_i+2)\ \cdots\ \mathbf{R}^T(k_i+m)\right]^T \tag{6a}$$

$$\tilde{R} = \begin{bmatrix} \mathbf{R}(k_i) & \mathbf{R}(k_i-1) & \cdots & \mathbf{R}(k_i-I+1) \\ \mathbf{R}(k_i+1) & \mathbf{R}(k_i) & \cdots & \mathbf{R}(k_i-I+2) \\ \vdots & \vdots & \ddots & \vdots \\ \mathbf{R}(k_i+m-1) & \mathbf{R}(k_i+m-2) & \cdots & \mathbf{R}(k_i+m-I+2) \end{bmatrix} \tag{6b}$$

$$\tilde{\Phi} = \left[\Phi_1\ \Phi_2\ \cdots\ \Phi_I\right]^T \tag{6c}$$

Notably, $k_i \approx I + (4 \sim 14)$ was suggested by Huang (2001) for a sample rate for measurement between 50 and 200 Hz. Such setting of k_i makes $\tilde{\mathbf{R}}$ exclude $\mathbf{R}(0)$, which is heavily affected by noise. Equation (5) normally represents a set of overdeterminant algebraic linear equations. Consequently, the coefficient matrices in the AR model are determined in a least-squares error sense,

$$\tilde{\Phi} = \left(\tilde{\mathbf{R}}^T\tilde{\mathbf{R}}\right)^{-1}\tilde{\mathbf{R}}^T\hat{\mathbf{R}} \tag{7}$$

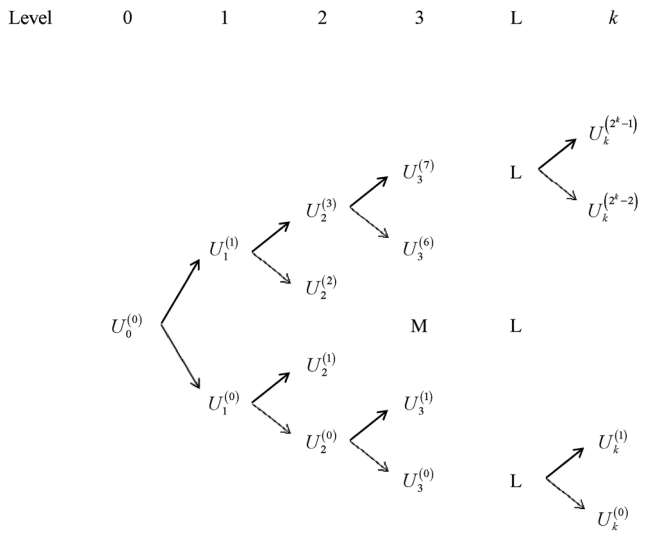

Fig. 1. Decomposition of subspaces.

2.2 Estimation of correlation functions in wavelet domain

The correlation functions are estimated from the measured responses by using the stationary wavelet packet transform. Owing to that the wavelet transform provides information in the time and frequency domains simultaneously, the correlation functions corresponding to the frequency range of interest can be constructed by selecting appropriate wavelets. Notably, the wavelet packet transform provides a richer decomposition and allows for better time–frequency localization of signals than the decomposition of signals by the discrete wavelet transform. The stationary wavelet packet transform is superior to the wavelet packet method in that the former is a translation–invariance transform, explaining its excellent computational efficiency for functions with time shift. Moreover, the stationary wavelet packet transform is implemented without down-sampling and maintains all of the elements in the coefficients across all of the decomposition levels.

Let the discrete signal $f(t)$ belong to the space $U_0^{(0)}$, it is decomposed into as many subspaces as needed and expressed as (Figure 1; Walden and Cristan, 1998; Fan and Zuo, 2006; Zhong and Oyadiji, 2007; Jiang and Adeli, 2004)

$$\begin{aligned} U_0^{(0)} &= U_1^{(0)} \oplus U_1^{(1)} \\ &= U_2^{(0)} \oplus U_2^{(1)} \oplus U_2^{(2)} \oplus U_2^{(3)} \\ &= \cdots \\ &= U_k^{(0)} \oplus U_k^{(1)} \oplus U_k^{(2)} \oplus \cdots \oplus U_k^{(2^k-2)} \oplus U_k^{(2^k-1)} \end{aligned} \tag{8}$$

where $\oplus$ denotes the direct sum of two subspaces; subscript k denotes the level of decomposition; and $U_{k-1}^{(2^{(k-1)}-n)}$ is decomposed into $U_k^{(2^k-2n+1)}$ and $U_k^{(2^k-2n)}$ with $n \le k$, and $U_k^{(i)} \perp U_k^{(j)}$ for $i \ne j$. Let

$$U_k^{(m)} = \text{closespan}\left\{\mu_{m,k,l}(t) = 2^{-k/2}\mu_m\left(2^{-k}(t-t_l)\right);\, l \in Z\right\} \tag{9}$$

where $t_l = l\Delta t$ and $\{\mu_{m,k,l}(t), l \in Z\}$ is a set of orthonormal basis functions for $U_k^{(m)}$. Because the measured signals are discrete, functions are expressed in discrete form. The basis functions satisfy

$$\begin{aligned} \left\langle \mu_{m,k,l}, \mu_{m,k,j} \right\rangle &= \Delta t \sum_{\bar{n} \in Z} \mu_{m,k,l}(t)\mu_{m,k,j}(t) \\ &= \begin{cases} 1 & \text{when} \quad l = j \\ 0 & \text{when} \quad l \ne j \end{cases} \end{aligned} \tag{10a}$$

$$\left\langle \mu_{m,k,l}(t), \mu_{n,i,j}(t) \right\rangle = 0 \text{ when } n \ne m \tag{10b}$$

Constructing the basis functions, begins with choosing a mother wavelet function $\psi(t)$ and the corresponding scale function $\phi(t)$. Let $\mu_0(t_{\bar{n}}) = \phi(t_{\bar{n}})$ and $\mu_1(t_{\bar{n}}) = \psi(t_{\bar{n}})$, then

$$\mu_{2m,k+1,l}(t) = \sqrt{2}\sum_{n \in Z} h_k[n]\,\mu_{m,k,l}(2t - t_n) \tag{11a}$$

$$\mu_{2m+1,k+1,l}(t) = \sqrt{2}\sum_{n \in Z} g_k[n]\,\mu_{m,k,l}(2t - t_n) \tag{11b}$$

where $h_0[n] = \langle \phi(t), \phi(2t - t_n) \rangle / \sqrt{2}$ and $g_0[n] = \langle \psi(t), \psi(2t - t_n) \rangle / \sqrt{2}$ are the low-pass filter and high-pass filter, respectively. The stationary wavelet packet transform is calculated in a similar manner as the wavelet packet transform, except that no decimation is performed after each filtering step (Fowler, 2005; Jose et al., 2008). The low-pass filter and high-pass at level $k+1$ are defined recursively as

$$h_{k+1}[n] = \begin{cases} h_k[n/2] & n \text{ even} \\ 0 & n \text{ odd} \end{cases};$$

$$g_{k+1}[n] = \begin{cases} g_k[n/2] & n \text{ even} \\ 0 & n \text{ odd} \end{cases}$$

Decomposing $f(t)$ for $l \in Z$ into subspaces $U_k^{(m)}$ with $m = 0, 1, 2, \ldots, 2^k - 1$, yields

$$f(t_{\bar{n}}) = \sum_{m=0}^{2^k-1}\sum_{l=0} a_{m,k,l}\mu_{m,k,l}(t_{\bar{n}}) \tag{12}$$

where $a_{m,k,l}$ refers to the stationary wavelet packet coefficients in subspace $U_k^{(m)}$ and

$$a_{m,k,l} = \left\langle f(t), \mu_{m,k,l}(t) \right\rangle \tag{13}$$

If $f_k^{(m)}(t)$ denotes the signals of $f(t)$ decomposed into subspace $U_k^{(m)}$, Equation (12) reveals that the frequency range of $f_k^{(m)}(t)$ depends only on the frequency range of $\mu_{m,k,l}(t)$. Notably, the stationary wavelet packet satisfies the translation–invariance property, leading to

$$f(t-t_n) = \sum_{m=0}^{2^k-1} \sum_{l=0} \bar{a}_{m,k,l} \mu_{m,k,l}(t)$$
$$\text{and} \quad \bar{a}_{m,k,l} = a_{m,k,l-n} \tag{14}$$

The correlation functions can be estimated by (Bendat and Piersol, 1993)

$$\mathbf{R}(k) = \frac{1}{L} \sum_{\bar{n} \in Z} \mathbf{y}(t_{\bar{n}}) \mathbf{y}^T(t_{\bar{n}} + t_k) \tag{15}$$

where $L = \bar{T}/\Delta t$ denotes the record length of measurement; $\mathbf{y}(t) = \mathbf{0}$ when $t < 0$ and $t > \bar{T}$, which occurs in the measured data. Using Equation (12),

$$\mathbf{y}(t) = \sum_{m=0}^{2^j-1} \sum_{l=0}^{L} \{a_{m,j,l}\} \mu_{m,j,l}(t) \tag{16}$$

Based on Equations (14) and (15), Equation (16) is rewritten as

$$\mathbf{R}(k) = \frac{1}{L} \sum_{\bar{n} \in Z} \left[\sum_{m=0}^{2^j-1} \sum_{l=0}^{L-k} \{a_{m,j,l}\} \mu_{m,j,l}(t_{\bar{n}}) \times \sum_{m=0}^{2^j-1} \sum_{l=0}^{L-k} \{a_{m,j,l+k}\}^T \mu_{m,j,l}(t_{\bar{n}}) \right] \tag{17}$$

By using the orthogonal properties given in Equation (10), Equation (17) is further simplified as

$$\mathbf{R}(k) = \frac{1}{L\Delta t} \sum_{m=0}^{2^j-1} \sum_{l=0}^{L-k} \{a_{m,j,l}\} \{a_{m,j,l+k}\}^T = \frac{1}{\bar{T}} \mathbf{R}_w(k) \tag{18}$$

where $\mathbf{R}_w(k) = \sum_{m=0}^{2^j-1} \sum_{l=0}^{L-k} \{a_{m,j,l}\} \{a_{m,j,l+k}\}^T$. To determine the coefficient matrices in the AR model from Equation (7), $\mathbf{R}(k)$ is replaced by $\mathbf{R}_w(k)$.

The stationary wavelet packet transform has fine filtering properties in frequency, which is highly effective in identifying the modal parameters of a structure. Using the signals in a specific subspace, for example, $U_j^{(\bar{m})}$, to estimate $\mathbf{R}_w(k)$ yields

$$\mathbf{R}_w(k) = \sum_{l=0}^{L-k} \{a_{\bar{m},j,l}\} \{a_{\bar{m},j,l+k}\}^T \tag{19}$$

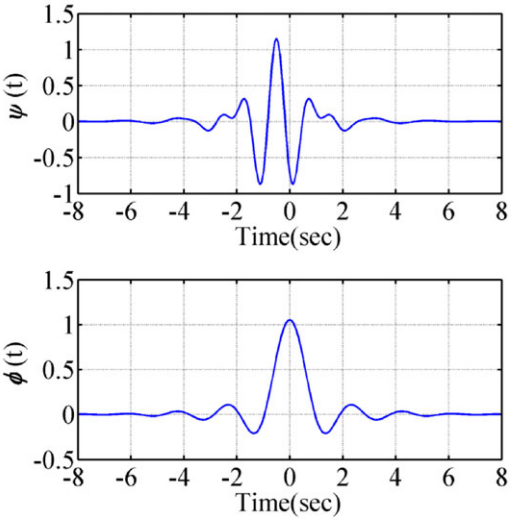

Fig. 2. Plots for Meyer mother wavelet $\psi(t)$ and corresponding scale function $\phi(t)$.

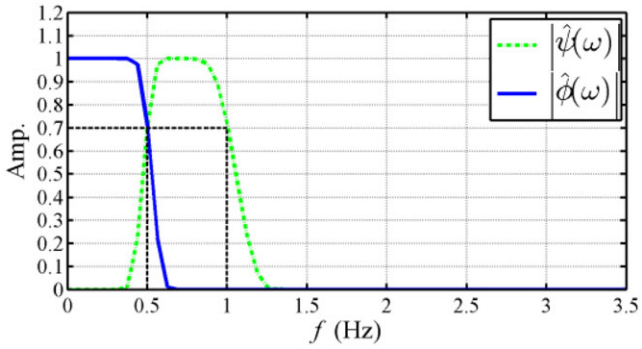

Fig. 3. Fourier spectra of Meyer wavelet and scale function.

If the Fourier transform of $\mu_{\bar{m},j,l}(t)$ has a compact support with the frequency range $[f_a, f_b]$, subspace $U_j^{(\bar{m})}$ corresponds to the frequency range $[f_a, f_b]$. Also, $\mathbf{R}_w(k)$ in Equation (19) is applied to Equation (7) to determine the coefficient matrices in the AR model and identify the natural frequencies of a structure by following the procedure given in Section 2.4. Doing so leads to the identified modal frequencies lying in the frequency range $[f_a, f_b]$.

2.3 Meyer stationary wavelet packets

The orthonormal basis functions in each subspace are constructed using Meyer mother wavelet $\psi(t)$ and its corresponding scale function $\phi(t)$ (Mallat, 1999) (Figure 2). Figure 3 shows the Fourier spectra of these two functions, $|\hat{\psi}(\omega)|$ and $|\hat{\phi}(\omega)|$, indicating that $\psi(t)$ is a band-pass filter and $\phi(t)$ is a low-pass filter.

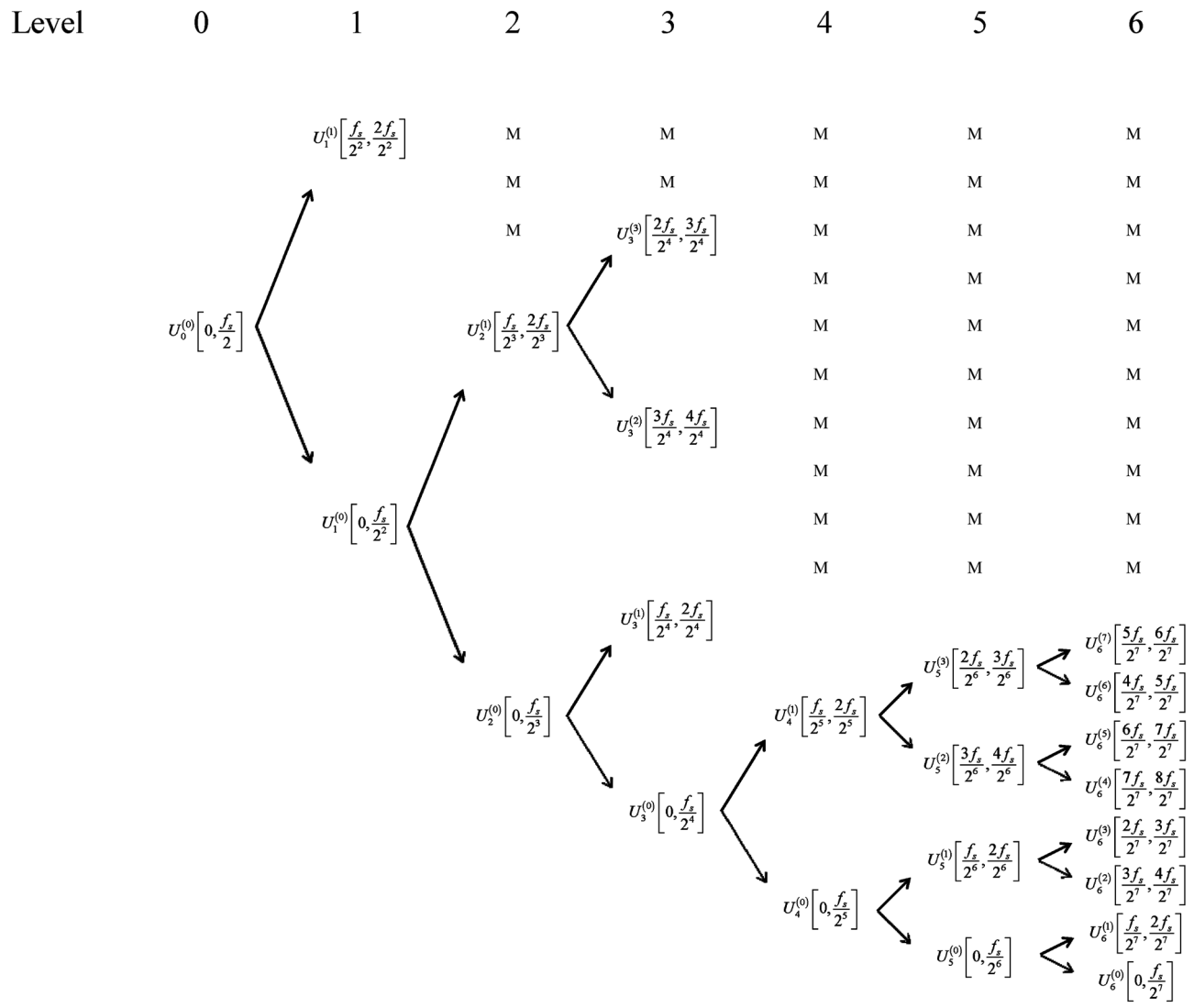

Fig. 4. Plots for Meyer mother wavelet $\psi(t)$ and corresponding scale function $\phi(t)$.

No overlapping frequency ranges among subspaces $U_k^{(m)}$ with different m allow for the convenient selection of an appropriate subspace to estimate the correlation function matrices through Equation (19) and identify the modal parameters of a structure in the frequency range of interest. In this work, the frequency ranges of $\psi(t)$ and $\phi(t)$ are defined by the frequency ranges corresponding to $50\sqrt{2}\%$ of $|\hat{\psi}(\omega)|$ and $|\hat{\phi}(\omega)|$, respectively, that is, [0.5, 1] Hz and [0, 0.5] Hz (Figure 3). Consequently, the frequency range of subspace $U_k^{(m)}$ is determined by the following procedure:

1. Express m in a vector of binary, $\mathbf{v} = (c_1, c_2, ..., c_{\bar{n}})$, where c_i is either 0 or 1.
2. Define a vector $\bar{\mathbf{v}} = \bar{c}_{\bar{n}} \otimes \bar{c}_{\bar{n}-1} \otimes \cdots \otimes \bar{c}_2 \otimes \bar{c}_1$, where $\otimes$ is the Kronecker tensor product operator, and $\bar{c}_i$ are set to (1, 1) and (1, −1) for $c_i = 0$ and 1, respectively. The components of $\bar{\mathbf{v}}$ are either −1 or 1.
3. Compute the number of zero crossing in the sequence of the components of $\bar{\mathbf{v}}$, and denote the number by η.
4. The frequency range of $U_k^{(m)}$ is $[\eta f_s/.2^{k+1}, (\eta+1) f_s/.2^{k+1}]$, where f_s is the sampling frequency.

For example, to find the frequency range of $U_3^{(6)}$, the binary expression of 6 is 110, $\mathbf{v} = (1, 1, 0)$, $\bar{\mathbf{v}} = [1, 1] \otimes [1, -1] \otimes [1, -1] = [1, -1, -1, 1, 1, -1, -1, 1]$, and $\eta = 4$. Thus, the frequency range of $U_3^{(6)}$ is $[4 f_s/2^3, 5 f_s/2^3]$. Figure 4 shows the frequency ranges of subspaces that may be used later.

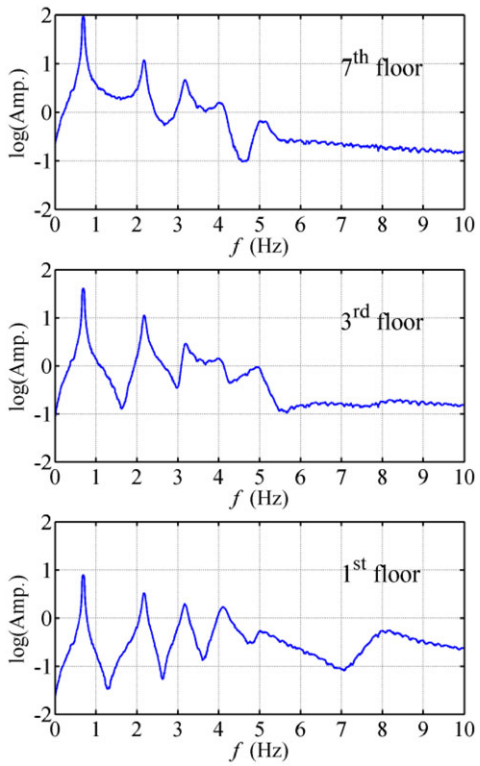

Fig. 5. Fourier spectra of simulated responses of first, third, and seventh floors.

2.4 Determination of modal parameters

By adopting the concept behind the Ibrahim time domain system identification approach, Yang et al. (1994) and Huang (1999) proved that the modal parameters of a structure can be directly determined from the eigenvalues and eigenvectors of the following matrix,

$$\mathbf{G} = \begin{bmatrix} \mathbf{0} & \mathbf{I} & \mathbf{0} & \mathbf{0} & \cdots & \mathbf{0} \\ \mathbf{0} & \mathbf{0} & \mathbf{I} & \mathbf{0} & \cdots & \mathbf{0} \\ \vdots & \vdots & \vdots & \vdots & \cdots & \vdots \\ \Phi_I & \Phi_{I-1} & \Phi_{I-2} & \Phi_{I-3} & \cdots & \Phi_1 \end{bmatrix}_{\bar{N}\times\bar{N}} \quad (20)$$

where $\mathbf{I}$ is an $\bar{l} \times \bar{l}$ unit matrix; $\bar{l}$ is the dimension of $\mathbf{y}(t)$, and $\bar{N} = I \times \bar{l}$.

Let λ_k and φ_k denote the kth eigenvalue and eigenvector of $\mathbf{G}$, respectively. The eigenvalue λ_k is normally a complex number, and is set to $\tilde{a}_k + i\tilde{b}_k$. The natural frequency and modal damping ratio of a structure are calculated by

$$\tilde{\beta}_k = \sqrt{\alpha_k^2 + \beta_k^2},\ \xi_k = -\alpha_k/\tilde{\beta}_k \quad (21)$$

where

$$\beta_k = \frac{1}{\Delta t}\tan^{-1}\left(\frac{\tilde{b}_k}{\tilde{a}_k}\right), \quad \alpha_k = \frac{1}{2\Delta t}\ln\left(\tilde{a}_k^2 + \tilde{b}_k^2\right) \quad (22)$$

The eigenvector $\boldsymbol{\varphi}_k$ can be expressed as $(\boldsymbol{\varphi}_{k1}^T\boldsymbol{\varphi}_{k2}^T...\boldsymbol{\varphi}_{kI}^T)^T$ where $\boldsymbol{\varphi}_{ki}$ has $\bar{l}$ components and satisfies $\boldsymbol{\varphi}_{ki} = \lambda_k\boldsymbol{\varphi}_{k(i-1)}$, and $\boldsymbol{\varphi}_{k1}$ corresponds to a mode shape of the measured degrees of freedom of a structure.

It is worthwhile to mention that spurious modes other than real structural modes occur when $\bar{N} > 2n$ where n is the total number of degrees of freedom of the structural system under consideration and is usually unknown. The real structural modes should consistently arise as I, that is, the order of the AR model, increases. Hence, the modal parameters of a structure can be determined based on the stabilization diagrams (Kullaa, 2000), which display the variations of the identified modal parameters with I. Good engineering judgment based on the knowledge of the structural system can be very helpful in identifying the structural modes.

3 NUMERICAL VERIFICATION

3.1 Determination of modal parameters

Numerically simulated velocity responses of a seven-storey shear building under base excitation of white noise input were processed to demonstrate the accuracy and effectiveness of the proposed approach in identifying the modal parameters. The theoretical natural frequencies of the shear building were 0.72, 2.21, 3.20, 4.11, 5.01, 5.26, and 8.01 Hz, and the corresponding modal damping ratios were 0.4%, 1.4%, 2.0%, 2.6%, 3.1%, 3.3%, and 5.0%. The responses of the shear building with a duration of 300 seconds were determined using the Runge–Kutta method with $\Delta t = 0.005$ seconds. Notably, the frequencies of the fifth and sixth modes are too close to be distinguished from the Fourier spectra in Figure 5.

The agreement between the identified and theoretical mode shapes is indicated by the modal assurance criterion (MAC) (Allemang and Brown, 1983),

$$\mathrm{MAC}(\bar{\boldsymbol{\varphi}}_{iI}, \bar{\boldsymbol{\varphi}}_{iA}) = \frac{\left|\bar{\boldsymbol{\varphi}}_{iI}^T\bar{\boldsymbol{\varphi}}_{iA}\right|^2}{\bar{\boldsymbol{\varphi}}_{iI}^T\bar{\boldsymbol{\varphi}}_{iI}\bar{\boldsymbol{\varphi}}_{iA}^T\bar{\boldsymbol{\varphi}}_{iA}} \quad (23)$$

where $\bar{\boldsymbol{\varphi}}_{iI}$ and $\bar{\boldsymbol{\varphi}}_{iA}$ are the identified and analytical ith mode shapes, respectively. The value of MAC is between zero and unity, and the closer to one of MAC indicates two mode shapes more similar.

For convenience, the identified results are considered as "accurate" when the identified frequencies and modal damping ratios are within 2% and 20% of the

Table 1
Identified modal parameters of a seven-floor shear building

Noise NSR	*Subspace (frequency range)*	*Orders of AR I*	*Modal frequencies f_n (Hz)*	*Damping ratios ξ (%)*	*MAC*
0%	$U_2^{(0)}$ (0 to 25 Hz)	2	0.72 (0%)	0.4 (0%)	1.00
			2.21 (0%)	1.4 (0%)	1.00
			3.20 (0%)	2.0 (0%)	1.00
			4.11 (0%)	2.5 (−3.85%)	1.00
			5.01 (0%)	3.2 (3.22%)	1.00
			5.26 (0%)	3.2 (−3.03%)	1.00
			8.00 (−0.12%)	5.0 (0%)	1.00
	$U_3^{(0)}$ (0 to 12.5 Hz)	2	0.72 (0%)	0.4 (0%)	1.00
			2.21 (0%)	1.4 (0%)	1.00
			3.20 (0%)	2.0 (0%)	1.00
			4.11 (0%)	2.5 (−3.85%)	1.00
			5.01 (0%)	3.4 (9.68%)	1.00
			5.25 (−0.19%)	3.3 (0%)	1.00
			8.03 (0.25%)	5.0 (0%)	1.00
20%	$U_3^{(0)}$ (0 to 12.5 Hz)	7	0.72 (0%)	0.4 (0%)	1.00
			2.21 (0%)	1.4 (0%)	1.00
			3.20 (0%)	2.0 (0%)	1.00
			4.12 (0.24%)	2.5 (−3.85%)	1.00
			5.01 (0%)	3.2 (3.23%)	1.00
			5.26 (0%)	3.5 (6.06%)	1.00
			7.99 (−0.25%)	4.8 (0%)	0.99
	$U_3^{(0)}$ (0 to 12.5 Hz)	2	0.72 (0%)	0.4 (0%)	1.00
			2.21 (0%)	1.4 (0%)	1.00
			3.20 (0%)	2.0 (0%)	1.00
			4.12 (0.24%)	2.5 (−3.84%)	1.00
	$U_3^{(0)}$ (4.70 to 6.25 Hz)	2	5.01 (0%)	2.6 (−16.13%)	1.00
			5.25 (−0.19%)	2.8 (−15.15%)	1.00
	$U_3^{(0)}$ (0 to 12.5 Hz)	2	7.97 (−0.50%)	5.2 (4%)	0.98

theoretical ones, respectively, and the MAC values exceed 0.9 as well. The identified natural frequencies are typically much more accurate than the identified modal damping ratios. Therefore, smaller errors are required for the identified natural frequencies than for identified modal damping ratios when defining accurate results.

Table 1 lists the identified modal parameters obtained using the responses of all floors. The relative differences between the identified results and true values are given in parentheses. The responses are transformed into different subspaces by the stationary wavelet packets. Highly accurate results are obtained using AR(2) and the signals in $U_2^{(0)}$ and $U_3^{(0)}$, whose frequency ranges are [0, 25] Hz and [0, 12.5] Hz, respectively.

3.2 Effects of noise and incomplete measurements

In real applications, the measured data always contain a certain level of corrupted noise. To simulate the noise effect, 20% variance of the noise-to-signal ratio (NSR) was randomly added to the computed responses. When the signals of all floors in subspace $U_3^{(0)}$ are employed to find the modal parameters, AR(I) models with $I \geq 7$ are needed to have accurate results, and the results using AR(7) are given in Table 1. The difficulties in accurately identifying modal parameters of the closed modes (fifth and sixth modes) result in using such large order of AR model. If the signals in subspace $U_6^{(2)}$, whose frequency range is [4.70, 6.25] Hz, are used for identifying the modes whose frequencies are inside the frequency range, Table 1 reveals that AR(2) yields accurate results, which are given in Table 1.

In practice, a highly dense sensor network is seldom used for measurement even with the increasingly cheap price of a monitoring system. Correspondingly, Table 2 summarizes the results obtained using the noisy responses of the first floor. The relative differences between the identified results and true values are given in

Table 2
Identified modal parameters of a seven-floor shear building using the noisy responses of the first floor

Present				*Randomdec Huang and Su (2007)*			
Subspace (frequency range)	*Orders of AR I*	f_n *(Hz)*	ξ *(%)*	*Scale factor in wavelet transform a (frequency range)*	*Orders of AR I*	f_n *(Hz)*	ξ *(%)*
$U_3^{(0)}$ (0 to 12.5 Hz)	50	/	/	1, 0.4, 0.3, 0.2 and 0.1 (0.5 to 10 Hz)	50	/	/
		2.41 (9.05%)	3.5 (150%)			2.32 (4.98%)	4.1 (193%)
		/	/			/	/
		4.06 (−1.22%)	4.0 (53.84%)			4.05 (−1.46%)	4.9 (88.46%)
		/	/			/	/
		/	/			/	/
		8.01 (0%)	4.5 (−10%)			8.13 (1.50%)	5.8 (16%)
$U_5^{(0)}$ (0 to 3.1 Hz)	10	0.72 (0%)	0.4 (0%)	1 (0.5 to 1 Hz)	8	0.72 (0%)	0.4 (0%)
		2.20 (−0.45%)	1.4 (0%)	0.4 (1.25 to 2.5 Hz)	11	2.21 (0%)	1.4 (0%)
$U_6^{(3)}$ (3.1 to 4.7 Hz)	10	3.20 (0%)	1.9 (−5%)	0.3 (1.66 to 3.33 Hz)	15	3.2 (0%)	1.9 (−5%)
		4.11 (0%)	2.5 (−3.84%)	0.2 (0.25 to 5 Hz)	12	4.12 (0.24%)	2.5 (−3.84%)
$U_6^{(2)}$ (4.7 to 6.25 Hz)	12	4.98 (−0.59%)	2.6 (−16.12%)	0.11 (4.54 to 9.09 Hz)	100	4.98 (−0.60%)	2.2 (−29.03%)
		5.24 (−0.38%)	3.5 (6.06%)			/	/
$U_5^{(3)}$ (6.25 to 9.4 Hz)	5	8.02 (0.12%)	4.5 (−10%)	0.1 (5 to 10 Hz)	9	8.08 (0.87%)	5.1 (2%)

Note: "/" denotes that the modes are not identified.

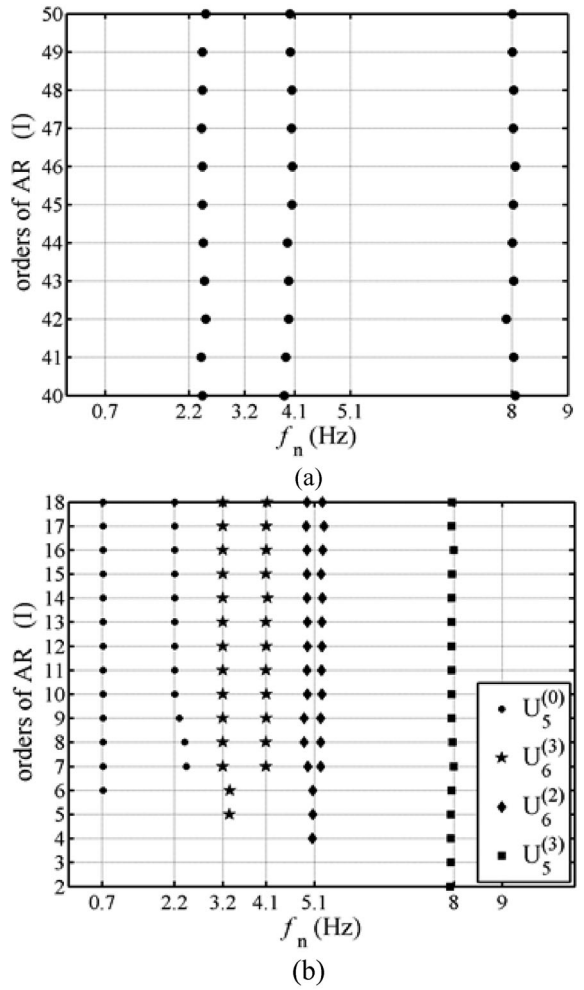

Fig. 6. Stabilization diagrams of identified frequencies for a seven-floor shear building: (a) using signals in $U_3^{(0)}$ only, (b) using signals in different subspaces for different modes.

parentheses. When the signals in subspace $U_3^{(0)}$ are used, even the AR(50) model does not yield accurate results for all of the modes. The stabilization diagram on frequencies given in Figure 6a shows that the frequencies of the first, third, fifth, and sixth modes are not identified when the order of AR model is less than 50 and demonstrates the difficulties of identifying accurate results of all modes from the signals in the subspace that covers the frequency range of all modes.

To resolve the above difficulties, different modes are identified using the signals in different subspaces. Table 2 demonstrates the feasibility of obtaining the accurate results of the first and second modes by using the AR(10) model in cooperation with the signals in $U_5^{(0)}$ that has a frequency range of [0, 3.1] Hz. Meanwhile, the AR(10) model along with the signals in $U_6^{(3)}$ with a frequency range of [3.1, 4.7] Hz yields accurate results of the third and fourth modes. Accurate results for the fifth and sixth modes can be obtained using the AR(12) model along with the signals in $U_6^{(2)}$ with a frequency range of [4.7, 6.25] Hz. Additionally, the AR(5) model along with the signals in $U_5^{(3)}$ with a frequency range of [6.25, 9.4] Hz yields accurate results for the seventh mode. According to the stabilization diagram in Figure 6, the real modes occur stably when increasing the orders of AR model, and no spurious modes are found in the frequency ranges of interest.

To compare the present approach with an existing approach, Table 2 also shows the results obtained using the approach of Huang and Su (2007), which combines the ARX model with the continuous wavelet transform, to process the Randomdec signatures extracted from the noisy responses using the random decrement technique. In processing the Randomdec signatures, which are equivalent to free decayed responses, the AR model, instead of the ARX model, should be used. Meyer wavelets were used in the wavelet transform, and a simple method proposed by Solís et al. (2013) was employed to avoid wavelet transform edge effects. When several values of scale parameter (a) in the continuous wavelet transform are applied to identify the modal parameters of all modes, similar to the present approach, the AR(50) model does not yield accurate results for all of the modes. When different values of a are used for identifying modal parameters of different modes, the AR(100) model does not give accurate result for the close modes (the fifth and sixth modes).

4 APPLICATIONS

Following its verification based on numerical simulation, the proposed approach is used to process the measured responses of an eight-storey, symmetrical steel frame under shaking table tests and ambient vibration responses of a cable-stayed bridge. In practical applications, the true modal parameters are unknown and the criteria given in the previous section for judging accurately identified results are inapplicable. However, real mechanical modes occur stably when increasing the order of AR model, whereas the spurious modes do not. The stabilization diagrams contribute to the evaluation of stable results. Modes identified at the current AR(I) are compared with the results obtained from the next six consecutive orders of AR (i.e., AR(I + k) and k = 1, 2,…,6). Importantly, the results are considered stable if (a) the maximum relative differences in frequency and damping ratio for each mode are less than 2% and 20%, respectively, and (b) the values of MAC are higher than 95%. Engineering judgment is

Fig. 7. A photo for an eight-storey steel frame under shaking table tests.

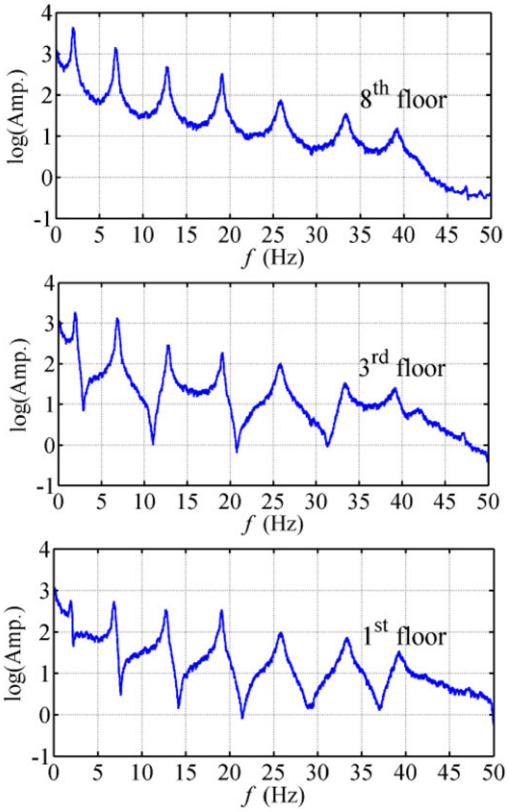

Fig. 8. Fourier spectra of the responses of an eight-storey steel frame at first, third, and eighth floors.

also highly effective in distinguishing real mechanical modes from spurious modes.

4.1 Eight-storey frame under shaking table tests

The eight-storey steel frame analyzed in this test was 1.5 m in length, 1.1 m in width, and 9.44 m in height (Figure 7). Lead plates of 250 kg were piled on each floor, such that the total mass of each floor was approximately 325 kg. The columns had H-shaped sections (H100×100×7.5×7.5). The frame was subjected to base excitation of white noise in long-span direction. A velocity sensor was placed at the center of each floor. The responses were recorded for 250 seconds with a sampling rate of 200 Hz.

Figure 8 displays the Fourier spectra of the responses at the first, third, and eighth floors, in which the peaks of the first seven modes under 40 Hz are clearly shown. Frequency of the eighth mode looks like that between 40 and 45 Hz (see the Fourier spectrum for the third floor). Table 3 lists the identified results obtained by using the signals of all floors in $U_1^{(0)}$, whose frequency range is [0, 50] Hz. The identified modal parameters appear stably when AR(I) with $I \geq 5$ are used. The parenthesized results in Table 3 are the natural frequencies obtained from the commercial finite element package, ETABS (2013), via the designed data. Following a typical way of applying ETABS to construct a finite element model for a real building, a 3D beam element was utilized to model a column in each storey, and rigid floor assumption was made. Apparently, the identified natural frequencies and those from ETABS significantly differ from each other, especially for the higher modes. Notably, the identified natural frequencies correspond very well with those associated with the peaks of the Fourier spectra in Figure 8. The values of MAC indicate the excellent correlation between the identified mode shapes and those of ETABS.

Table 3 also summarizes the identified results using the responses of the first floor only, whereas Figure 9 depicts the stabilization diagrams on frequencies obtained from signals in different subspaces. When the signals in $U_1^{(0)}$ are used, Figure 9a reveals that AR(I) with $I \geq 32$ are needed to obtain stable results for all of the eight modes. Some spurious modes occur in the frequency range of interest, causing difficulty in determining the modal parameters precisely. The identified natural frequencies and modal damping ratios closely correspond to those obtained from complete

Table 3
Identified modal parameters of an eight-storey steel frame under shaking table tests

Responses	*Subspace (frequency range)*	f_n *(Hz)*	ξ *(%)*	*MAC*
All floors	$U_1^{(0)}$ (0 to 50 Hz)	2.11 (2.01)	1.4	0.99
		7.00 (6.49)	0.9	0.99
		12.86 (12.38)	0.7	0.99
		19.15 (19.80)	0.4	0.99
		25.89 (26.46)	0.9	0.97
		33.42 (34.36)	1.0	0.97
		39.36 (44.84)	1.3	0.96
		41.63 (56.80)	2.1	0.96
First floor only	$U_1^{(0)}$ (0 to 50 Hz)	2.09	4.0	/
		6.97	0.8	/
		12.85	0.7	/
		19.15	0.4	/
		25.89	0.9	/
		33.42	1.0	/
		39.32	1.0	/
		42.34	2.5	/
	$U_3^{(0)}$ (0 to 12.5 Hz)	2.06	1.3	/
		6.98	0.9	/
	$U_3^{(1)}$ (12.5 to 25.5 Hz)	12.85	0.7	/
		19.15	0.4	/
	$U_3^{(3)}$ (25.5 to 37.5 Hz)	25.89	0.9	/
		33.42	0.9	/
	$U_3^{(2)}$ (37.5 to 50 Hz)	39.35	0.9	/
		41.60	2.1	/

Note: "/" denotes data not available.

measurements, except for the damping ratios of the first mode.

When the modal parameters of different modes are identified using the signals in different subspaces, Figure 9b reveals that a markedly smaller order of AR model than that for using the signals in $U_1^{(0)}$ (see Figure 9a) is needed to achieve stable results; no spurious modes occur in the frequency ranges of

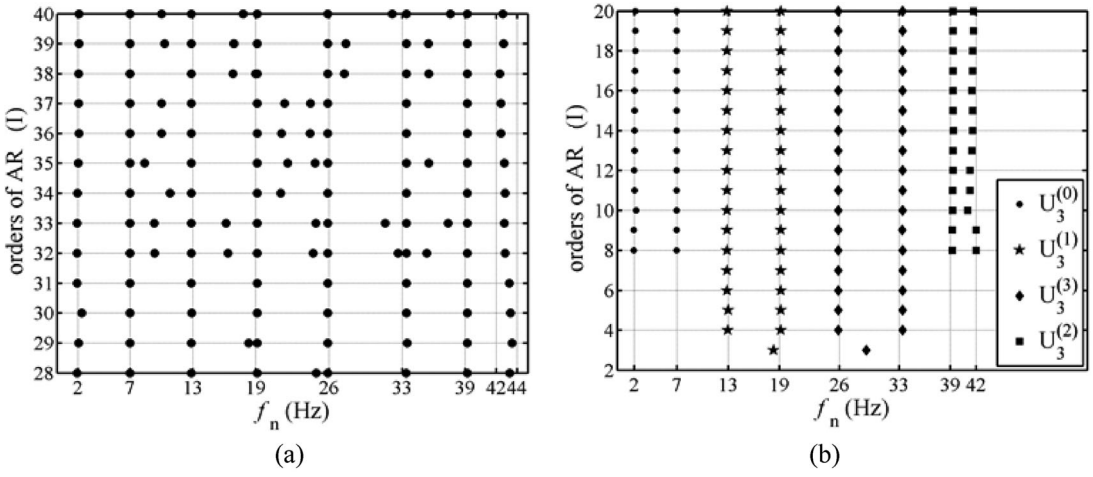

Fig. 9. Stabilization diagrams of identified frequencies for an eight-storey steel frame using the responses of the first floor only: (a) using signals in $U_1^{(0)}$ only, (b) using signals in different subspaces for different modes.

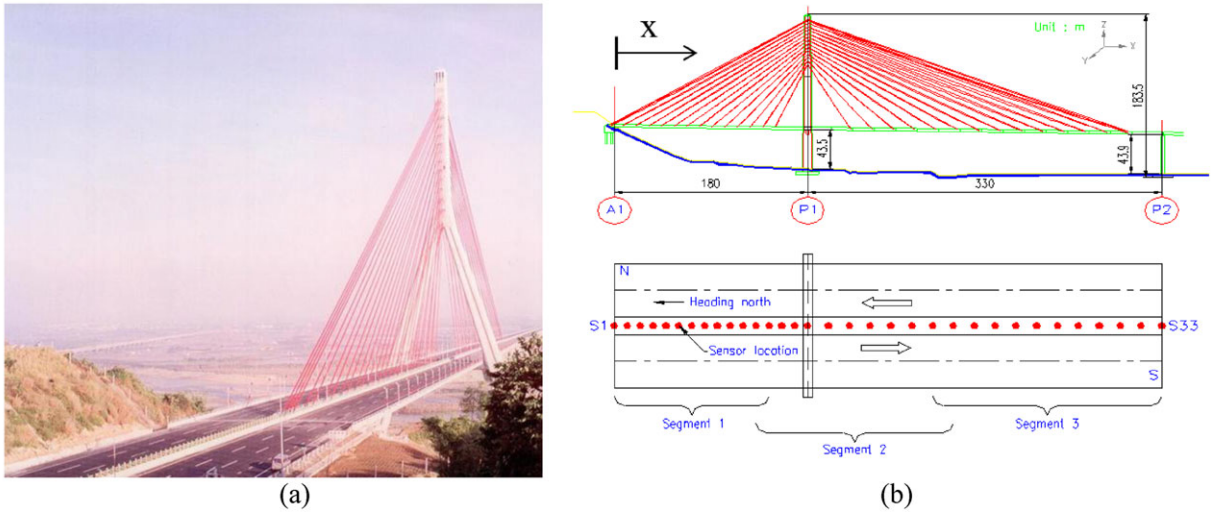

Fig. 10. (a) A photo of the cable-stayed bridge (provided by Taiwan Area National Expressway Engineering Bureau), (b) sensor layout for ambient vibration measurement.

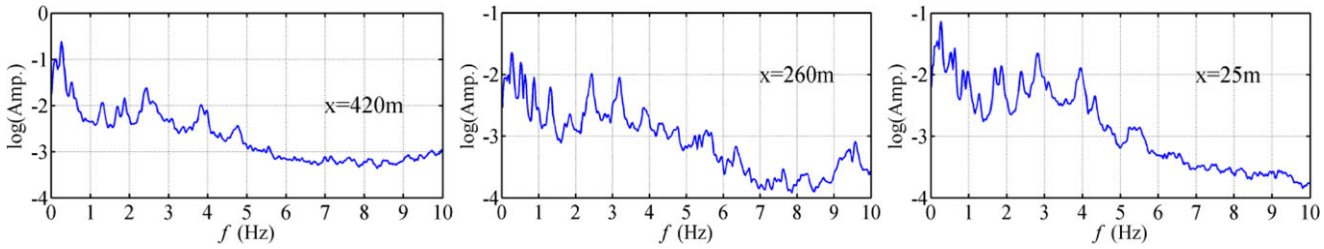

Fig. 11. Fourier spectra of vertical responses at $x = 25$, 260, and 420 m.

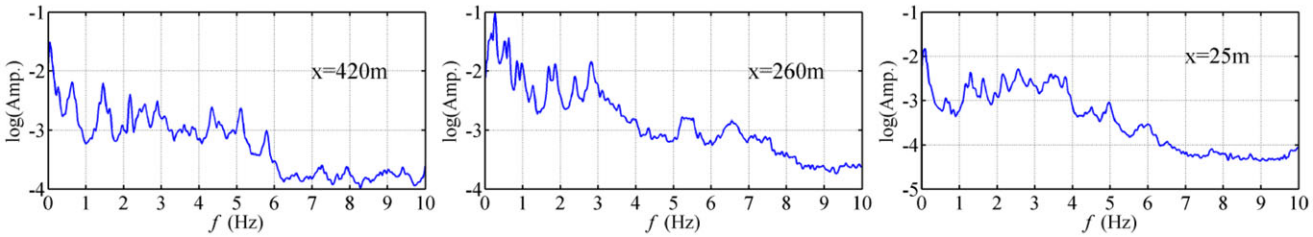

Fig. 12. Fourier spectra of transverse responses at $x = 25$, 260, and 420 m.

interest. The identified modal parameters are consistent with those obtained from complete measurements (Table 3).

4.2 Ambient vibration of a cable-stayed bridge

In a second example, the proposed approach was used to process the ambient vibrations of a highway cable-stayed bridge, which is the largest spanned bridge in Taiwan (Figure 10). The bridge has a deck of 34.5 m in width, a main span of 330 m with a steel box girder type of deck, a side span of 180 m with a prestressed concrete box girder type of deck, and an inverted Y-shaped reinforced concrete pylon of 183.5 m in height. Each side of the pylon has 14 pairs of cables. The back stays consist of four cables, and the other stays have two cables. Thirty-three measuring stations were arranged along the centerline of the bridge deck to measure the ambient vibrations. Most of the stations were located near the connections of cables to the deck. Owing to the limited number of sensitive servo-velocity sensors, the tested bridge was divided into three segments (Figure 10). Two overlapping stations for any two adjacent segments were utilized to correlate the

Table 4
Identified modal parameters of a cable-stayed bridge from ambient vibration responses

	Present				*Chen & Ou (2011)*		
Direction	*Subspace (frequency range)*	f_n *(Hz)*	ξ *(%)*	*MAC*	f_n *(Hz)*	ξ *(%)*	*MAC*
Vertical	$U_3^{(0)}$ (0 to 6.25 Hz)	0.27 (0.29)	2.6	1	0.28	2.9	1
		0.59 (0.56)	2.5	1	0.57	3.7	0.98
		0.90 (0.93)	2.6	1	0.92	4.4	0.97
		1.58 (1.52)	2.7	1	1.54	3.9	0.97
		1.86 (1.79)	2.6	0.97	1.81	3	0.97
		2.36 (2.52)	2.5	1	/	/	/
		3.11 (3.27)	2.9	0.99	/	/	/
		3.93 (4.02)	2.7	0.98	/	/	/
Transverse	$U_3^{(0)}$ (0 to 6.25 Hz)	0.65 (0.65)	2.6	1	0.64	3.3	0.99
		1.64 (1.68)	2.7	1	1.64	2.9	0.99
		2.19 (2.15)	2.4	1	2.17	3.2	0.99
		2.57 (2.49)	2.9	1	2.51	2.5	0.99
		3.17 (3.15)	2.6	0.99	3.13	3.9	0.99
		3.89 (3.95)	2.8	1	/	/	/

Note: "/" denotes data not available.

mode shapes identified for each segment. Responses in the vertical and transverse directions were measured separately. The ambient vibration responses of the bridge were recorded for 10 minutes with a sampling rate of 100 Hz.

Figures 11 and 12 display the Fourier spectra of the measured ambient vibrations at some stations in vertical and transverse directions, respectively. Because most of the peaks in the Fourier spectra occur in frequencies smaller than 5 Hz, the modes with frequencies under 4 Hz were identified using the proposed approach. Because the different segments were not measured simultaneously, the measured responses in different segments were processed separately.

Table 4 lists the average values of natural frequencies and modal damping ratios obtained from measured responses in three segments. The modal parameters were identified using the signals in subspace $U_3^{(0)}$ with a frequency range of [0, 6.25] Hz. Figures 13 and 14 show the identified mode shapes in vertical and transverse directions, respectively. Cumulatively, eight modes in vertical direction and six modes in transverse direction were identified. The stable results were determined by using AR(14). The parenthesized results in Table 4 are the natural frequencies obtained from the commercial finite element package, SAP2000 (2013), via the designed data with some modifications in supports and connections suggested by Chen and Ou (2011). The finite element model consisted of 33 and 38 beam elements for the deck and the pylon, respectively, and 28 cable elements for the stay cables. The MAC values refer to the correlation between the identified mode shapes and those from the finite element analysis. Figures 13 and 14 also show the vertical and transverse mode shapes obtained from the finite element method, respectively. The identified natural frequencies correlate well with the finite element results, whereas the identified mode shapes closely correspond to those from the finite element analysis with MAC values larger than 0.97.

For comparison, Table 4 also lists the identified results of Chen and Ou (2011), who applied the approach of Huang and Su (2007) to process the Randomdec signatures extracted from the ambient vibration responses. They identified five modes in both of the vertical and transverse directions. The mode shapes are also given in Figures 13 and 14. The MAC values refer to the correlation between the mode shapes identified by the present approach and those of Chen and Ou (2011). The natural frequencies and mode shapes of Chen and Ou (2011) show excellent agreement with those obtained from the present approach, whereas reasonable agreement is found for most of the modal damping ratios.

For a situation in which only the responses of a station were processed, Table 5 lists the identified mode parameters using the responses at $x = 260$ m in the second segment. Again, the results were obtained using the signals in different subspaces in wavelet domain cooperating with AR modes having different orders. Figures 15 and 16 show the stabilization diagrams of identified frequencies in vertical and transverse directions, respectively. The excellent agreement between

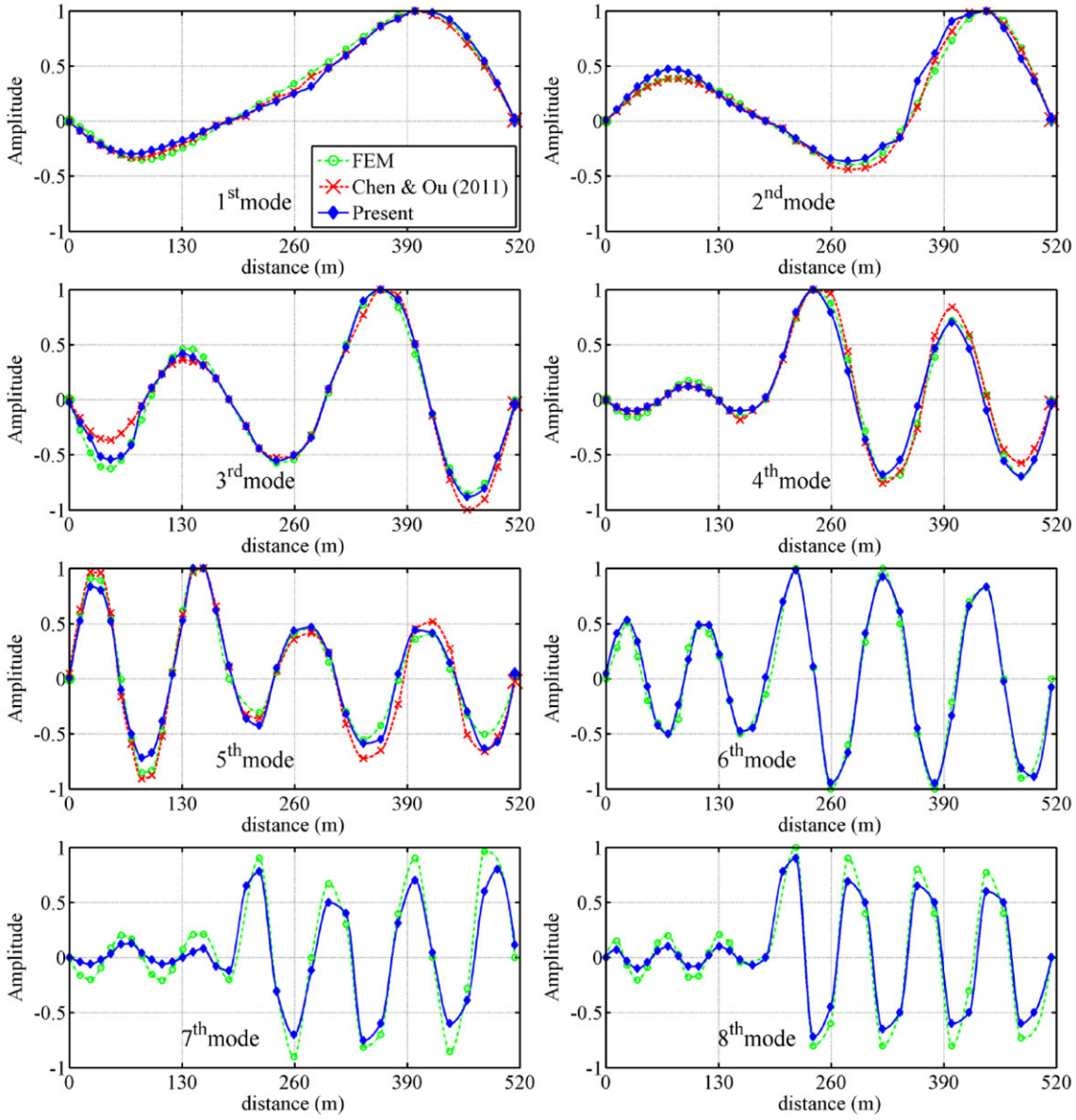

Fig. 13. Mode shapes in vertical direction.

the modal parameters in Tables 4 and 5 again indicates the ability of the proposed approach to accurately find the natural frequencies and damping ratios of many modes from responses of very few degrees of freedom. Figures 15a and 16a reveal some spurious modes whose frequencies are near the natural frequencies. Additionally, when the signals in subspace $U_3^{(0)}$ are used to determine the modal parameters listed in Table 5, the AR(I) model with $I \geq 31$ is required to obtain stable results. Again, using signals in different subspaces to identify different modes eliminates the spurious modes and substantially reduces the needed orders of AR model to obtain stable results (Figures 15b and 16b).

5 CONCLUDING REMARKS

This work has developed a wavelet-based approach for identifying the modal parameters of a structure from its ambient vibration responses. The stationary wavelet packet transform is applied to the ambient vibration responses, and the correlation functions between measured degrees of freedom can be estimated using the signals in the subspaces in the wavelet domain. Modal parameters of the structure are then determined from the coefficient matrices of the AR model, which are established using those correlation functions. Compared to the discrete wavelet transform and

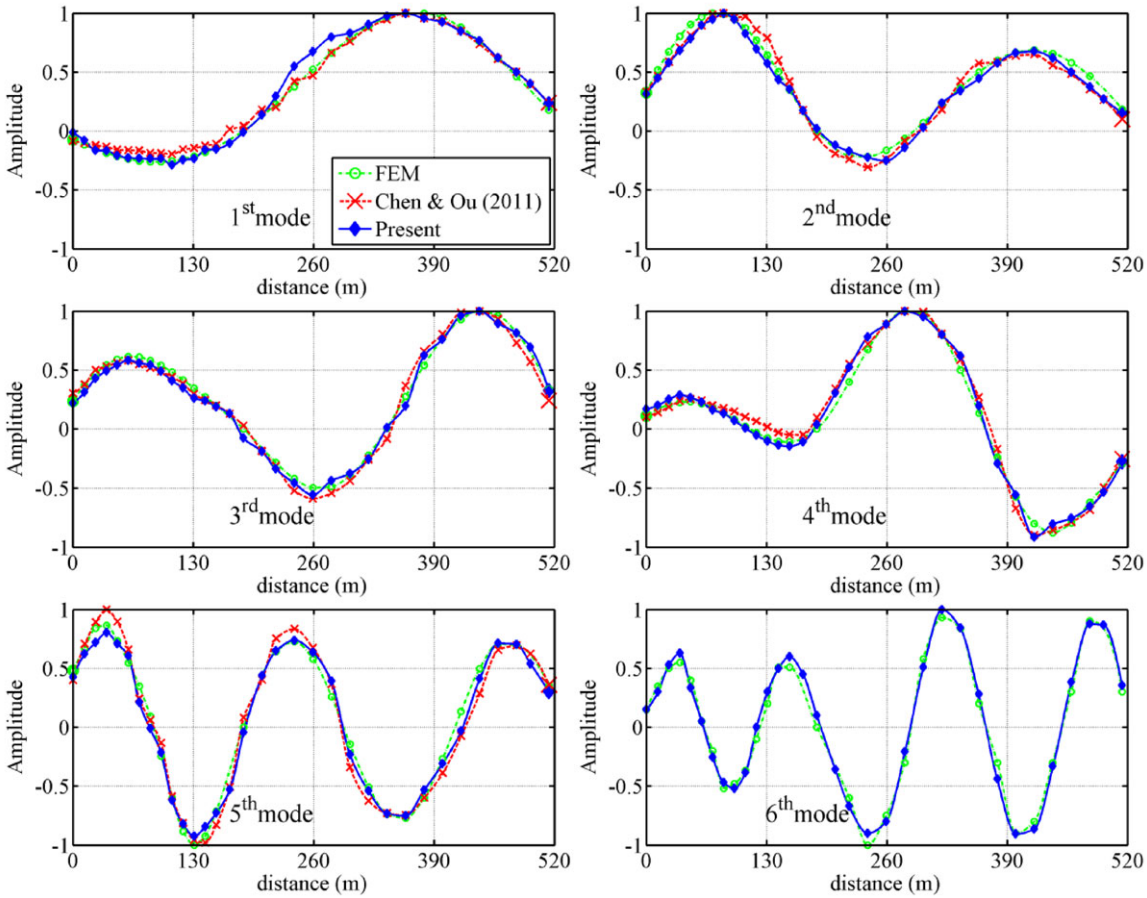

Fig. 14. Mode shapes in transverse direction.

Table 5
Identified modal parameters of a cable-stayed bridge using ambient vibration responses of a station only

Direction	*Subspace (frequency range)*	f_n *(Hz)*	ξ *(%)*
Vertical	$U_5^{(0)}$ (0 to 1.55 Hz)	0.27	2.5
		0.58	2.7
		0.89	2.4
	$U_5^{(1)}$ (1.55 to 3.13 Hz)	1.56	2.9
		1.86	2.8
		2.35	2.7
		3.10	2.9
	$U_5^{(3)}$ (3.13 to 4.7 Hz)	3.90	2.9
Transverse	$U_4^{(0)}$ (0 to 3.13 Hz)	0.66	2.5
		1.61	2.6
		2.18	2.7
		2.58	2.8
	$U_4^{(1)}$ (3.13 to 6.25 Hz)	3.17	2.8
		3.89	2.6

wavelet packet transform, the stationary wavelet packet transform satisfies the translation invariance property and saves the computational time in constructing the correlation functions. The Meyer wavelets were used in the proposed approach because Meyer mother wavelet is a band-pass filter, and the corresponding scale function is a low-pass filter. The fine filtering properties in the stationary wavelet packet transform enhance the ability of proposed approach to identify both the closely spaced modes and many modes from the responses of very few measured degrees of freedom.

The present approach was validated first by successfully processing the numerically simulated velocity responses of a seven-storey shear building with closely spaced modes of the fifth and sixth modes under base excitation of white noise. Natural frequencies and modal damping ratios of the seven modes were identified easily and accurately even when the responses of only one degree of freedom with 20% noise were used.

To demonstrate the applicability of the proposed approach to process the real measured data, this work also analyzed the velocity responses of an eight-storey steel frame under shaking table tests and the ambient vibration responses of a highway cable-stayed bridge subjected to traffic flow. Eight modes of the steel frame and

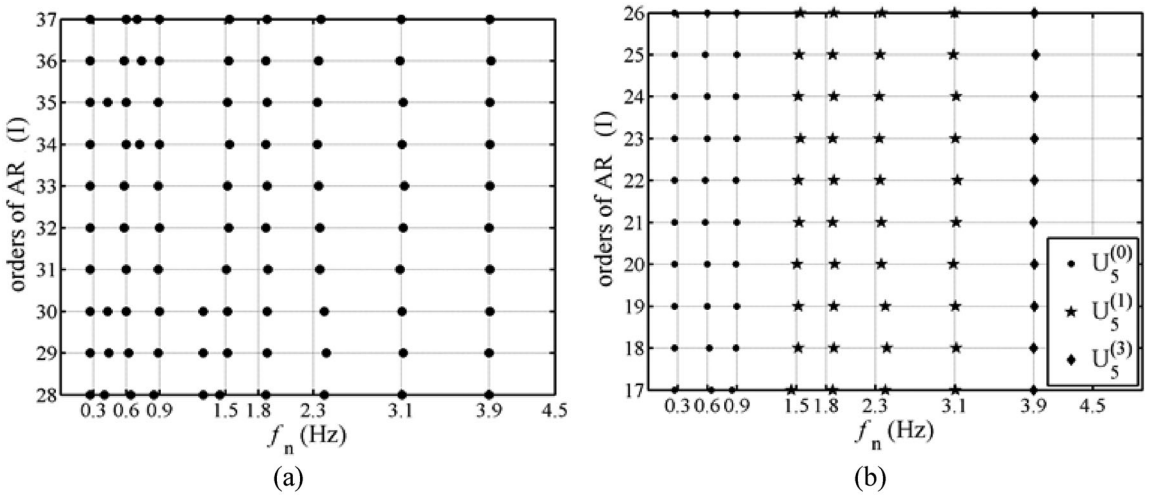

Fig. 15. Stabilization diagrams of identified frequencies for a cable-stayed bridge using the vertical responses at $x = 260$ m: (a) using signals in $U_3^{(0)}$ only, (b) using signals in different subspaces for different modes.

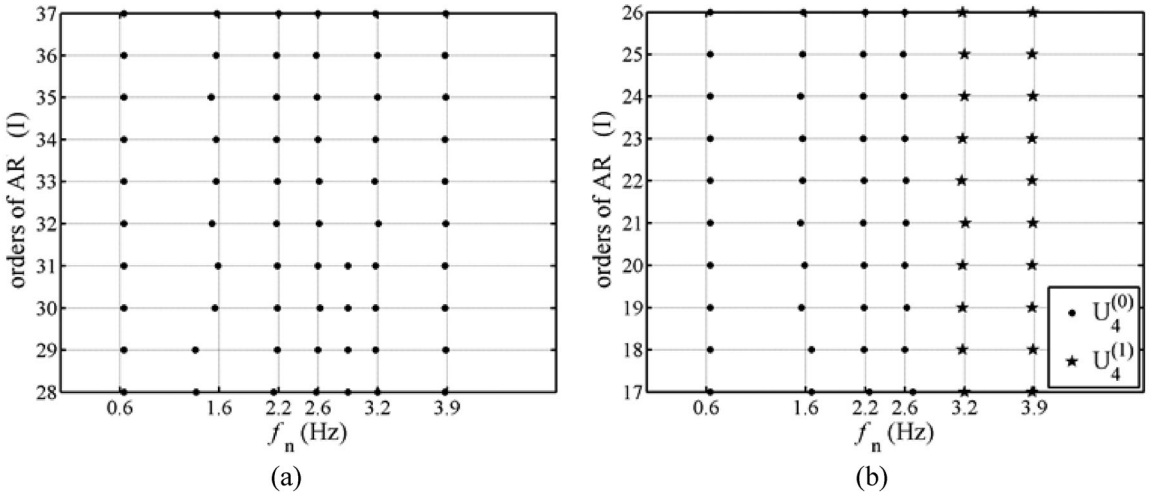

Fig. 16. Stabilization diagrams of identified frequencies for a cable-stayed bridge using the transverse responses at $x = 260$ m: (a) using signals in $U_3^{(0)}$ only, (b) using signals in different subspaces for different modes.

eight modes in vertical direction and six modes in transverse direction of the bridge were identified even when the measured responses of only one degree of freedom were used.

During the processing of the numerically simulated responses and measured responses, our results indicate two main advantages of using signals in different subspaces in wavelet domain to identify different modes over using signals in a subspace to identify all of the modes. Those advantages are that the AR mode with markedly lower order is needed and that spurious modes occur to a lesser extent. Importantly, the proposed approach can identify the natural frequencies and modal damping ratios of many modes from the responses of only one degree of freedom. The capacity is highly useful for long-term structural health monitoring using vibration-based approaches in a cost-effective manner.

ACKNOWLEDGMENTS

The authors would like to thank the National Science Council of the Republic of China, Taiwan, for financially supporting this research under Contract No. NSC 101–2625-M-009–007. The appreciation is also extended to the National Center for Research on Earthquake Engineering for providing shaking table test data.

REFERENCES

Adeli, H. & Jiang, X. (2006), Dynamic fuzzy wavelet neural network model for structural system identification, *Journal of Structural Engineering*, **132**(1), 102–11.

Adeli, H. & Jiang, X. (2009), *Intelligent Infrastructure— Neural Networks, Wavelets, and Chaos Theory for Intelligent Transportation Systems and Smart Structures*, CRC Press, Taylor & Francis, Boca Raton, FL.

Adeli, H. & Saleh, A. (1997), Optimal control of adaptive/smart bridge structures, *Journal of Structural Engineering*, **123**(2), 218–26.

Ali, M. R. & Okabayashi, T. (2011), System identification of highway bridges from ambient vibration using subspace stochastic realization theories, *Earthquake and Structures*, **2**(2), 189–206.

Allemang, R. L. & Brown, D. L. (1983), A correlation coefficient for modal vector analysis, in *Proceedings of the 1st International Modal Analysis Conference*, Bethel, CT, 110–16.

Bendat, J. S. & Piersol, A. G. (1993), *Engineering Applications of Correlation and Spectral Analysis*, 2nd edn. John Wiley & Sons, New York.

Brown, D., Allemang, R., Zimmerman, R. & Mergay, M. (1976), Parameter estimation techniques for modal analysis, *SAE Transactions*, **88**(1), 828–46.

Caicedo, J. M. (2011), Practical guidelines for the natural excitation technique (NExT) and the eigensystem realization algorithm (ERA) for modal identification using ambient vibration, *Experimental Techniques*, **35**(4), 52–58.

Chen, C. H. & Ou, C. I. (2011), Experimental model test and time-domain aerodynamic analysis of a cable-stayed bridge, *International Journal of Structural Stability and Dynamics*, **11**(1), 101–25.

Chen, J., Zuo, M. J., Zi, Y., He, Z., Yuan, J. & Chen, X. (2013), Customized lifting multiwavelet packet information entropy for equipment condition identification, *Smart Materials and Structures*, **22**(9), 095022.

Cole, H. A., Jr. (1971), *Methods and apparatus for measuring the damping characteristics of a structure*, United States Patent No. 3620069.

Dionysius, M. & Yozo, F. (2007), System identification of suspension bridge from ambient vibration response, *Engineering Structures*, **30**(2), 462–77.

EATABS (2013), *Integrated Analysis, Design and Drafting of Building Systems*, Computers & Structures, Inc., Berkeley, CA.

Fan, X. & Zuo, M. J. (2006), Gearbox fault detection using Hilbert and wavelet packet transform, *Mechanical Systems and Signal Processing*, **20**(4), 966–82.

Fowler, J. (2005), The redundant discrete wavelet transform and additive noise, *Signal Processing Letters, IEEE*, **12**(9), 629–32.

García-Palencia, A. J. & Santini-Bell, E. (2013), A two-step model updating algorithm for parameter identification of linear elastic damped structures, *Computer-Aided Civil and Infrastructure Engineering*, **28**(7), 509–21.

Gouttebroze, S. & Lardies, J. (2001), On using the wavelet transform in modal analysis, *Mechanics Research Communications*, **28**(5), 561–69.

Hazra, B. & Narasimhan, S. (2010), Wavelet-based blind identification of the UCLA Factor building using ambient and earthquake responses, *Smart Materials and Structures*, **19**(4), 1–10.

Hazra, B., Sadhu, A., Roffel, A. J. & Narasimhan, S. (2012), Hybrid time-frequency blind source separation towards ambient system identification, *Computer-Aided Civil and Infrastructure Engineering*, **27**(5), 314–32.

He, X., Moaveni, B., Conte, J. P. & Elgamal, A. (2008), Modal identification study of Vincent Thomas bridge using simulated wind-induced ambient vibration data, *Computer-Aided Civil and Infrastructure Engineering*, **23**(5), 373–88.

Hsu, W.Y. (2013), Single-trial motor imagery classification using asymmetry ratio, phase relation and wavelet-based fractal features, and their selected combination, *International Journal of Neural Systems*, **23**(2), 1350007.

Hu, X.Y., Wang, B. & Ji, H. (2013), A wireless sensor network-based structural health monitoring system for highway bridges, *Computer-Aided Civil and Infrastructure Engineering*, **28**(3), 193–209.

Huang, C. S. (1999), A study on techniques for analyzing ambient vibration measurement (II)—time series methods. *Report No. NCREE-99–018, National Center for Research on Earthquake Engineering,* Taipei, Taiwan (in Chinese).

Huang, C. S. (2001), Structural identification from ambient vibration measurement using the multivariate AR model, *Journal of Sound and Vibration*, **241**(3), 337–59.

Huang, C. S., Hung, S. L., Lin, C. I. & Su, W. C. (2005), A wavelet-based approach to identifying structural modal parameters from seismic response and free vibration data, *Computer-Aided Civil and Infrastructure Engineering*, **20**(6), 408–23.

Huang, C. S. & Lin, H. L. (2001), Modal identification of structures from ambient vibration, free vibration, and seismic response data via a subspace approach, *Earthquake Engineering and Structural Dynamics*, **30**(12), 1857–78.

Huang, N. E., Shen, Z., Long, S. R., Wu, M. C., Shih, H. H., Zheng, Q., Yen, N. C., Tung, C. C. & Liu, H. H. (1998), The empirical mode decomposition and Hilbert spectrum for nonlinear and nonstationary time series analysis, *Proceedings of the Royal Society A-Mathematical Physical and Engineering Sciences*, **454**(1971), 903–95.

Huang, C. S. & Su, W. C. (2007), Identification of modal parameters of a time invariant linear system by continuous wavelet transformation, *Mechanical Systems and Signal Processing*, **21**(4), 1642–64.

Huang, C. S. & Yeh, C. H. (1999), Some properties of Randomdec signatures, *Mechanical Systems and Signal Processing*, **13**(3), 491–506.

Hung, S. L., Huang, C. S., Wen, C. M. & Hsu, Y. C. (2003), Nonparametric identification of a building structure from experimental data using wavelet neural network, *Computer-Aided Civil and Infrastructure Engineering*, **18**(5), 358–70.

Ibrahim, S. R. & Mikulcik, E. C. (1973), A time domain modal vibration test technique, *Shock and Vibration Bulletin*, **43**(4), 21–37.

Ibrahim, S. R. & Pappa, R. S. (1982), Large modal survey testing using the Ibrahim time domain identify technique, *The AIAA Journal of Spacecraft and Rockets*, **19**(5), 459–65.

Jiang, X. & Adeli, H. (2004), Wavelet packet-autocorrelation function method for traffic flow pattern analysis, *Computer-Aided Civil and Infrastructure Engineering*, **19**(5), 324–37.

Jiang, X. & Adeli, H. (2005), Dynamic wavelet neural network for nonlinear identification of highrise buildings, *Computer-Aided Civil and Infrastructure Engineering*, **20**(5), 316–30.

Jiang, X. & Adeli, H. (2007), Pseudospectra, MUSIC, and dynamic wavelet neural network for damage detection

of highrise building, *International Journal for Numerical Methods in Engineering*, **71**(5), 606–29.
Jiang, X. & Adeli, H. (2008), Dynamic fuzzy wavelet neuroemulator for nonlinear control of irregular highrise building structures, *International Journal for Numerical Methods in Engineering*, **74**(7), 1045–66.
Jiang, X., Mahadevan, S. & Adeli, H. (2007), Bayesian wavelet packet denoising for structural system identification, *Structural Control and Health Monitoring*, **14**(2), 333–56.
Jose Perez-Solano, J., Felici-Castell, S. & Rodriguez-Hernandez, M. A. (2008), Narrowband interference suppression in frequency-hopping spread spectrum using undecimated wavelet packet transform, *IEEE Transactions on Vehicular Technology*, **57**(3), 1620–29.
Kang, N., Kim, H., Choi, S., Jo, S., Hwang, J. S. & Yu, E. (2012), Performance evaluation of TMD under typhoon using system identification and inverse wind load estimation, *Computer-Aided Civil and Infrastructure Engineering*, **27**(6), 455–73.
Kodogiannis, V. S., Amina, M. & Petrounias, I. (2013), A clustering-based fuzzy-wavelet neural network model for short-term load forecasting, *International Journal of Neural Systems*, **23**(5), 1350024.
Kougioumtzoglou, I. A. & Spanos, P. D. (2013), An identification approach for linear and nonlinear time-variant structural systems via harmonic wavelets, *Mechanical Systems and Signal Processing*, **37**(1–2), 338–52.
Kullaa, J. (2000), System identification of Heritage Court Tower using stochastic subspace method, in *Proceedings of the* 18th *International Modal Analysis Conference*, San Antonio, TX, 1088–94.
Lardies, J. (2010), Modal parameter identification based on ARMAV and state-space approaches, *Archive of Applied Mechanics*, **80**(4), 335–52.
Lardies, J. & Gouttebroze, S. (2002), Identification of modal parameters using the wavelet transform, *International Journal of Mechanical Sciences*, **44**(11), 2263–83.
Lardies, J. & Ta, M. N. (2011), Modal parameter identification of stay cables from output-only measurements, *Mechanical System and Signal Processing*, **25**(1), 133–150.
Lin, C. M., Ting, A. B., Hsu, C. F. & Chung, C. M. (2012), Adaptive control for MIMO uncertain nonlinear systems using recurrent wavelet neural network, *International Journal of Neural Systems*, **22**(1), 37–50.
Liu, T. Y., Chiang, W. L., Chen, C. W., Hsu, W. K., Lu, L. C. & Chu, T. J. (2011), Identification and monitoring of bridge health from ambient vibration data, *Journal of Vibration and Control*, **17**(4), 589–603.
Ljung, L. (1999), *System Identification: Theory for the User*, 2nd edn, Prentice Hall, Upper Saddle River, NJ.
Loh, C. H. & Wu, T. S. (1996), Identification of Fei-Tsui arch dam from both ambient and seismic response data, *Soil Dynamics and Earthquake Engineering*, **15**(7), 465–83.
Lozano-Galant, J. A., Nogal, M., Castillo, E. & Turmo, J. (2013), Application of observability techniques to structural-system identification, *Computer-Aided Civil and Infrastructure Engineering*, **28**(6), 343–450.
Mallat, S. (1999), *A Wavelet Tour of Signal Processing*, 2nd edn, Academic, San Diego, CA.
Mcneill, S. I. (2011), An analytic formulation for blind modal identification, *Journal of Vibration and Control*, **18**(4), 2111–21.
Osornio-Rios, R. A., Amezquita-Sanchez, J. P., Romero-Troncoso, R. J. & Garcia-Perez, A. (2012), MUSIC-neural network analysis for locating structural damage in truss type structures by means of vibrations, *Computer-Aided Civil and Infrastructure Engineering*, **27**(9), 687–98.
Robertson, A. N., Park, K. C. & Alvin, K. F. (1998), Extraction of impulse response data via wavelet transform for structural system identification, *Journal of Vibration and Acoustics*, **120**(1), 252–60.
Ruzzene, M., Fasana, A., Garibalidi, L. & Piombo, B. (1997), Natural frequencies and dampings identification using wavelet transform: application to real data, *Mechanical Systems and Signal Processing*, **11**(3), 207–18.
SAP2000 (2013), *Integrated Software for Structural Analysis & Design*, Computers & Structures, Inc., Berkeley, CA.
Schoenwald, D. A. (1993), System identification using a wavelet-based approach, in *Proceedings of the 32nd IEEE Conference on Decision and Control*, San Antionio, TX, 3064–65.
Schoukens, J. & Pintelon, R. (1991), *Identification of Linear Systems: A Practical Guide to Accurate Modeling*, Pergamon Press, Oxford.
Sirca, G. F., Jr. & Adeli, H. (2012), System identification in structural engineering, *Scientia Iranica –Transaction A: Civil Engineering*, **19**(6), 1355–64.
Solís, M., Algeba, M. & Galvín, P. (2013), Continuous wavelet analysis of mode shapes differences for damage detection, *Mechanical Systems and Signal Processing*, **40**(2), 645–66.
Soyoz, S. & Feng, M. Q. (2009), Long-term monitoring and identification of bridge structural parameters, *Computer-Aided Civil and Infrastructure Engineering*, **24**(2), 82–92.
Vandiver, J. K., Dunwoody, A. B., Campbell, R. B. & Cook, M. F. (1982), A mathematical basis for the random decrement vibration signature analysis technique, *Journal of Mechanical Design*, **104**(2), 307–13.
Vold, H. & Russell, R. (1983), Advanced analysis methods improve modal test results, *Sound and Vibration*, **17**(3), 36–40.
Walden, A. T. & Cristan, A. C. (1998), The phase-corrected undecimated discrete wavelet packet transform and its application to interpreting the timing of events, *Proceedings of the Royal Society of London, A-Mathematical Physical and Engineering Sciences*, **454**(1976), 2243–66.
Wang, Z. N. & Fang, T. (1986), A time domain method for identifying modal parameters, *Journal of Applied Mechanics*, **53**(1), 28–32.
Yan, B. & Miyamoto, A. (2006), A comparative study of modal parameter identification based on wavelet and Hilbert-Huang transforms, *Computer-Aided Civil and Infrastructure Engineering*, **21**(1), 9–23.
Yan, W. J. & Ren, W. X. (2012), Operational modal parameter identification from power spectrum density transmissibility, *Computer-Aided Civil and Infrastructure Engineering*, **27**(3), 202–17.
Yang, J. N., Lei, Y. & Huang, N. (2004), Identification of natural frequencies and damping of in situ tall buildings using ambient wind vibration data, *Journal of Engineering Mechanics*, **130**(5), 570–77.
Yang, Q. J., Zhang, P. Q., Liand, C. Q. & Wu, X. P. (1994), A system theory approach to multi-input multi-output modal parameters identification method, *Mechanical Systems and Signal Processing*, **8**(2), 159–74.

Yuen, K.V. & Katafygiotis, L.S. (2006), Substructure identification and health monitoring using response measurement only, *Computer-Aided Civil and Infrastructure Engineering*, **21**(4), 280–91.

Zhong, S. & Oyadiji, S. O. (2007), Crack detection in simply-supported beams without baseline modal parameters by stationary wavelet transform, *Mechanical Systems and Signal Processing*, **21**(4), 1853–84.

Zhou, W. & Chelidze, D. (2007), Blind source separation based vibration mode identification, *Mechanical System and Signal Processing*, **21**(8), 3072–87.